processes

MDPI

Article

New Porous Silicon-Containing Organic Polymers: Synthesis and Carbon Dioxide Uptake

Safaa H. Mohamed [1], Ayad S. Hameed [1], Emad Yousif [2,*], Mohammad Hayal Alotaibi [3,*], Dina S. Ahmed [4] and Gamal A. El-Hiti [5,*]

1 Department of Chemistry, College of Science, Tikrit University, Tikrit 34001, Iraq; safaaketmeer@gmail.com (S.H.M.); ch@sc.nahrainuniv.edu.iq (A.S.H.)
2 Department of Chemistry, College of Science, Al-Nahrain University, Baghdad 64021, Iraq
3 National Center for Petrochemicals Technology, King Abdulaziz City for Science and Technology, Riyadh 11442, Saudi Arabia
4 Department of Medical Instrumentation Engineering, Al-Mansour University College, Baghdad 64021, Iraq; dinasaadi86@gmail.com
5 Cornea Research Chair, Department of Optometry, College of Applied Medical Sciences, King Saud University, Riyadh 11433, Saudi Arabia
* Correspondence: emad_yousif@hotmail.com (E.Y.); mhhalotaibi@kacst.edu.sa (M.H.A.); gelhiti@ksu.edu.sa (G.A.E.-H.); Tel.: +966-11469-3778 (G.A.E.-H.); Fax: +966-11469-3536 (G.A.E.-H.)

Received: 15 October 2020; Accepted: 17 November 2020; Published: 18 November 2020

Abstract: The design and synthesis of new multifunctional organic porous polymers has attracted significant attention over the years due to their favorable properties, which make them suitable for carbon dioxide storage. In this study, 2-, 3-, and 4-hydroxybenzaldehyde reacted with phenyltrichlorosilane in the presence of a base, affording the corresponding organosilicons **1–3**, which further reacted with benzidine in the presence of glacial acetic acid, yielding the organic polymers **4–6**. The synthesized polymers exhibited microporous structures with a surface area of 8.174–18.012 m^2 g^{-1}, while their pore volume and total average pore diameter ranged from 0.015–0.035 cm^3 g^{-1} and 1.947–1.952 nm, respectively. In addition, among the synthesized organic polymers, the one with the *meta*-arrangement structure **5** showed the highest carbon dioxide adsorption capacity at 323 K and 40 bar due to its relatively high surface area and pore volume.

Keywords: carbon dioxide storage; adsorption; porous organic polymers; Schiff base; polysilicates

1. Introduction

Fossil fuels are under pressure due to the constantly increasing energy demand in many industrial applications. However, their combustion leads to high levels of greenhouse gas (e.g., carbon dioxide (CO_2)) emissions [1], which in turn cause several environmental problems including weather changes and global warming [2]. Therefore, the capture of CO_2 plays a vital role in reducing the negative effects of global warming [3–6]. The efficient capture and storage of CO_2 requires its separation from other gases, such as hydrogen (H_2), methane (CH_4), and nitrogen (N_2), which can be achieved under high-pressure conditions during pre-combustion or at atmospheric pressure and temperature during post-combustion [7]. The storage process involves the adsorption of CO_2 followed by desorption of the gas in a pure form.

To date, the commercial scale processes for the separation of CO_2 from gas flue have mainly focused on the use of amines, aqueous ammonia, and potassium carbonate as absorbents [8,9]. Although the use of chilled ammonia is simple and easy and generates ammonium carbonate as a solid at a relatively low temperature (<20 °C) [9], the process requires significantly high energy levels. Alternatively,

a mixture of polyethylene glycol and dimethyl ether has been used as a CO_2 absorbent [10], as it requires low energy for the generation step. However, this method is suitable only for streams with high pressure. Ionic liquids also require low energy for the solvent regeneration and can absorb CO_2 through physisorption [11], but have high viscosity, which limits the absorption rate of CO_2 [12]. In contrast, solid CO_2 adsorbents are more beneficial in terms of energy efficiency compared to absorbents, as they can form van der Waals (physisorption) or covalent (chemisorption) bonds with CO_2 [13].

Porous materials, such as activated carbons, zeolites, molecular sieves, and metal oxides, are common CO_2 physical adsorbents [14] and their properties can be easily modified by incorporating several functional groups [15]. In particular, porous materials should have low density and high CO_2 adsorption capacity, surface area, and physical and chemical stability under practical conditions [16]. Porous organic polymers (POPs) have high CO_2 adsorption efficiency and stability in harsh environments, well-defined structure of porous networks, good lifetime, and recyclability, which make them suitable materials for gas storage [17]. Hence, the development of new POPs as gas storage media, heterogeneous catalysts, molecular sensors, light harvesters, and other applications has recently attracted considerable attention [18–25]. POPs can be synthesized either through simple, convenient, and high yielding synthetic procedures or by using suitable monomers [18], which may bear multifunctional groups that lead to high-porosity materials with different geometries [26–30]. For example, MCM-41, produced from pulverized coal fly ash, has a large pore volume and acts as an excellent CO_2 storage medium in the presence of amine [31]. The implementation of both strategies allows full control of both the functionality and the porosity of the synthesized POPs. Furthermore, it has been reported that porous polymeric materials with tetrahedral geometry have a high surface area, porosity, rigidity, and gas adsorption capacity [32–37].

In this regard, our group has recently designed, synthesized, and examined the application of various materials as gas storage media [38–43]. Herein, we synthesized a series of new polymeric materials that contain silicon and a Schiff base moiety to investigate their properties and applicability as CO_2 storage media. Specifically, three silicon-containing polymers were successfully prepared with a porous amorphous surface and different particle diameters. Further characterizations revealed that all polymers were thermally stable at temperatures of up to 400 °C and could reversibly adsorb CO_2 within their pores. Finally, the estimation of the CO_2 uptake by the three polymers revealed that their pore size distribution, surface area, and geometry could significantly affect their CO_2 storage capacity.

2. Materials and Methods

2.1. Instrumentation

The FTIR and ^{1}H NMR spectra (500 MHz) were recorded on a Shimadzu 8400 spectrophotometer (Shimadzu, Tokyo, Japan) and a Bruker DRX500 NMR spectrometer (Bruker, Zürich, Switzerland), respectively. Energy dispersive X-ray spectroscopy was analyzed on a Bruker XFlash 610. The field emission scanning electron microscopy (FESEM) images were obtained using a SIGMA 500 VP microscope (ZEISS Microscopy, Jena, Germany), while the X-ray powder diffraction (XRD) spectra were measured on an ADX-2500 X-ray diffraction instrument (Angstrom Advanced, Inc., Stoughton, MA, USA). The thermogravimetric analysis (TGA) was performed on a TGA4000 thermogravimetric analyzer (PerkinElmer, Waltham, MA, USA) and the differential scanning calorimetry (DSC) analysis was carried out on an ASTM E1356 calorimeter (Intertek, Wilton UK). A Quantchrome analyzer was used to record the nitrogen (N_2) adsorption–desorption isotherms at 77 K, while the surface area and pore sizes were calculated using the Brunauer–Emmett–Teller (BET) method. The pore volumes were determined at a relative pressure ($p/p°$) of 0.98. The CO_2 uptake was estimated on an H-sorb 2600 high-pressure volumetric adsorption analyzer (Gold APP Instrument Corporation, Beijing, China) at 323 K and 40 bar. Before the measurements, the polymers were dried at 150 °C under inert atmosphere (N_2) for 5 h and degassed at 50 °C under dynamic vacuum for 1 h. A standard procedure was used for

the preparation of sample for adsorption experiments and the samples were sputter coated by gold (ca. 15 nm).

*2.2. Synthesis of Organosilicons **1–3***

To a stirred solution of 2-, 3-, or 4-hydroxybenzaldehyde (3.66 g, 30 mmol) in dry pyridine (20 mL) at 0 °C under nitrogen atmosphere, a solution of phenyltrichlorosilane (2.11 g, 10 mmol) in dry tetrahydrofuran (THF; 10 mL) was added dropwise over 30 min through a dropping funnel. The mixture was stirred at 40–45 °C for 6 h and then was allowed to cool to room temperature. The generated solid was removed by filtration and washed with THF (3 × 25 mL). The filtrate was then concentrated under reduced pressure, affording a yellow oil, which was washed with cold distilled water (2 × 10 mL) and dried under reduced pressure at 60 °C for 2 h to give the corresponding organosilicon **1**, **2**, or **3**.

*2.3. Synthesis of Polymers **4–6***

A mixture of **1**, **2**, or **3** (4.65 g, 10 mmol) and benzidine (2.76 g, 15 mmol) in THF (25 mL) containing glacial acetic acid (AcOH; 0.5 mL) was stirred under reflux for 5 h under nitrogen atmosphere. The mixture was allowed to cool to room temperature, generating a solid, which was afterwards filtered, washed with THF (2 × 10 mL) and hexane (3 × 10 mL), and dried under reduced pressure for 2 h to give the corresponding polymer **4**, **5**, or **6** as an orange powder.

3. Results

*3.1. Synthesis of Organosilicons **1–3***

The reaction of 2-, 3-, and 4-hydroxybenzaldehyde with phenyltrichlorosilane in pyridine as a base at 40–45 °C for 6 h afforded the desired [(phenylsilanetriyl)*tris*(oxy)]tribenzaldehydes **1–3** as yellow oils in 73–85% yields (Scheme 1).

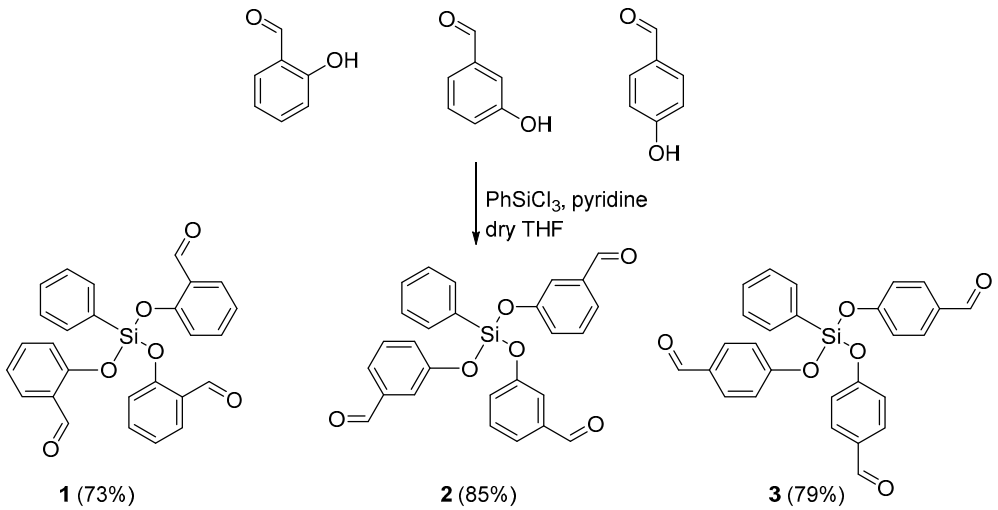

Scheme 1. Synthesis of organosilicons **1–3**.

A strong absorption band was observed at 1686–1713 cm^{-1} in the FTIR spectra of **1–3** (Figures S1–S3), which was attributed to the aldehyde carbonyl group, while no absorption band corresponding to the hydroxyl group of the hydroxybenzaldehydes was detected, implying the effective reaction of the starting aldehydes. The formation of the desired organosilicons was confirmed by the appearance of the characteristic peak of the Si–O group at 1161–1174 cm^{-1}. The most common FTIR absorption bands detected for **1–3** are reported in Table 1.

Table 1. Common FTIR absorption bands of organosilicons **1–3**.

Organosilicon	FTIR (ν, cm^{-1})				
	C–H	C = O	C = C	Si–O	C–O
1	3010	1686	1599	1161	1136
2	3036	1709	1587	1174	1155
3	3077	1713	1612	1167	1142

Moreover, a singlet peak was observed at 9.93–9.91 μmol/mol in each of the ^{1}H NMR spectra of **1–3** (Figures S4–S6), which corresponded to the protons of the aldehyde groups, while the protons of the aromatic moieties were also detected (Table 2). In particular, the structure of **2** was further confirmed by the ^{13}C NMR spectroscopic data (Figure S7), where a very strong peak was observed at 191.3 μmol/mol, corresponding to the carbonyl group of aldehyde, while all the expected aromatic carbons were identified within the 153.9–116.8 μmol/mol region.

Table 2. ^{1}H NMR data of organosilicons **1–3**.

Organosilicon	^{1}H NMR (500 MHz: DMSO-d_6, δ, μmol/mol, J in Hz)
1	9.93 (*s*, 3H, 3 × CHO), 7.54–7.39 (*m*, 5H, Ph), 7.11–6.96 (*m*, 12H, Ar)
2	9.92 (*s*, 3H, 3 × CHO), 7.81–7.72 (*m*, 5H Ph), 7.61–7.32 (*m*, 12H, Ar)
3	9.91 (*s*, 3H, 3 × CHO), 7.89–7.80 (*m*, 5H, Ph), 7.74 (*d*, J = 8.3 Hz, 6H, Ar), 7.62 (*d*, J = 8.3 Hz, 6H, Ar)

3.2. Synthesis of Polymers ***4–6***

The reaction of **1–3** and benzidine in boiling THF in the presence of glacial acetic acid for 5 h gave the corresponding polymers **4–6** in 79–85% yields (Scheme 2). The FTIR spectra of **4–6** (Figures S8–S10) indicated the absence of the carbonyl group, clearly implying the polymerization of **1–3**. Additional absorption bands were also detected with the 1605–1647 cm^{-1} region, which were attributed to the azomethane bond (C=N). The most common FTIR absorption bands of **4–6** and their melting points, yields, and color are shown in Table 3.

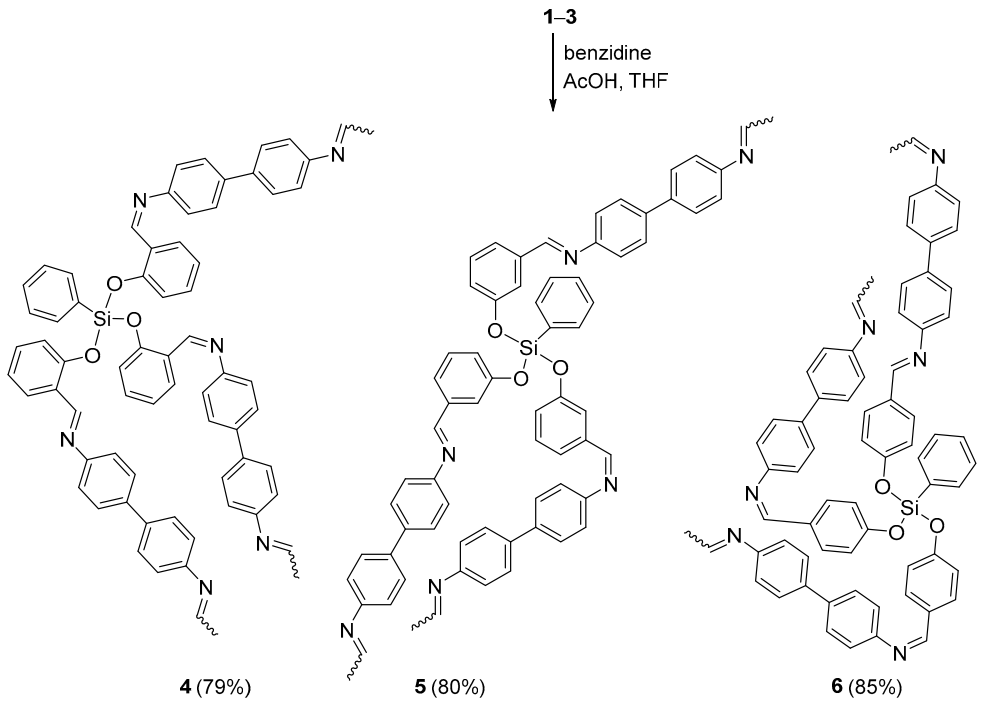

Scheme 2. Synthesis of **4–6**.

Table 3. Common FTIR absorption bands of **4–6** and their melting points, yields and color.

Polymer	Melting Point (°C)	Yield (%)	Color	FTIR (ν, cm^{-1})		
				C = N	C = C	Si–O
4	261–265	79	Light yellow	1605	1572	1169
5	286–291	80	Light brown	1647	1584	1173
6	246–250	85	Dark yellow	1626	1580	1113

To further confirm the formation of the desired polymers, the elemental composition of **4–6** was determined by energy-dispersive X-ray spectroscopic measurements (Figures S11–S13), indicating the presence of carbon, nitrogen, oxygen, and silicon in 84.4–85.6, 6.5–7.1, 6.5–7.0, and 1.0–1.5%, respectively.

3.3. *Surface Morphology of Polymers* ***4–6***

The FESEM technique provides not only less distorted, but also high-resolution pictures for the surface of the examined material [44]. Thus, it was used in this study to explore the surface morphology of the synthesized polymers **4–6** (Figure 1 and Figures S14–S16).

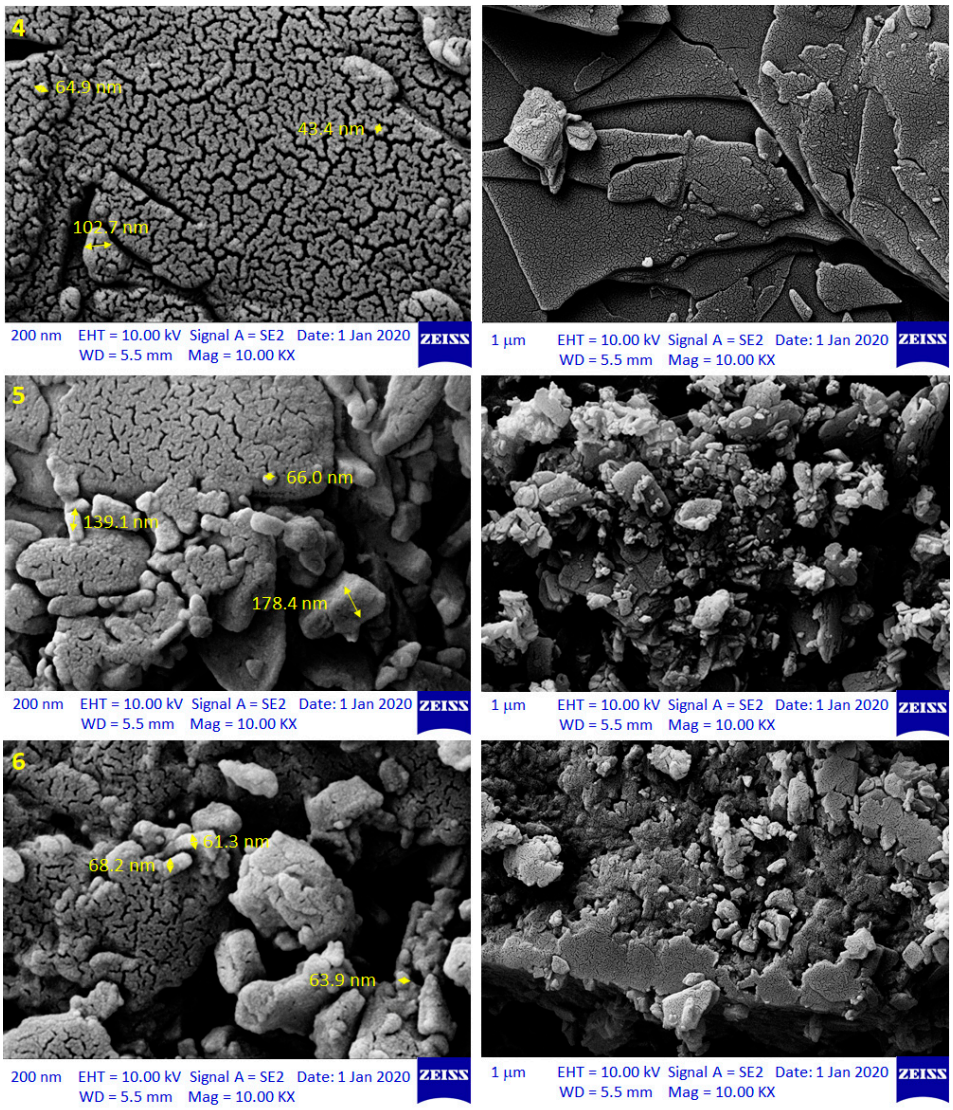

Figure 1. Field emission scanning electron microscopy (FESEM) images of polymers **4–6**.

In particular, the FESEM images shown in Figure 1 indicated that **4–6** were porous materials and irregular in shape, uniform, and contained cracks within smoother surfaces. However, despite their similar surface morphology, the particles within the surface had different shape, size, and diameter. Specifically, the particle diameter of polymers **4**, **5**, and **6** was 35.3–109.8, 40.2–178.4, and 45.2–208.2 nm, respectively.

The X-ray powder diffraction was also used to examine the surface of the synthesized polymers **4–6**, as it can provide useful information about the crystallinity, defects, average grain size, and strain of the examined material [45]. As shown in Figure 2, polymers **4–6** had amorphous and very similar structures, which contained an aura that was described as a broad hump. There was no degree of any crystalline form within the polymeric structure. The amorphous structure could result from the sliding of the layers, which destructed the crystalline forms. It should also be noted that there were no peaks indicating a specific recurring shape within the structures.

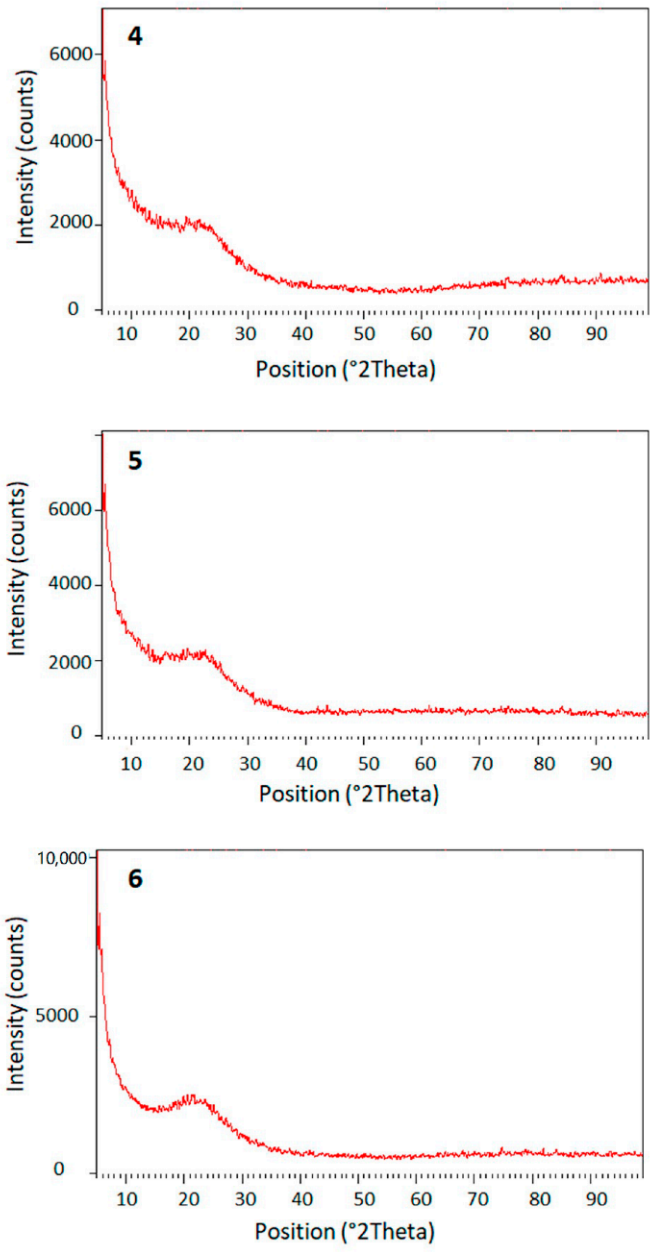

Figure 2. Powder XRD pattern of polymers **4–6**.

3.4. TGA and DSC of Polymers ***4–6***

TGA is mainly used to explore the thermal stability and composition of polymers [46]. When the temperature rises, polymers may lose weight, and volatile components, such as low molecular weight oligomers, moisture, or residual solvents, can be abstracted. It is also known that the degradation of polymers at high temperatures leads to the formation of volatile components due to chain scission, elimination of side groups, and unzipping to monomers [47,48]. Thus, the weight loss of the synthesized polymeric materials could be estimated by TGA.

Figure 3 shows a significant weight loss was observed between 285 °C and 400 °C (Table 4), suggesting that the polymers **4–6** consisted of only one phase due to the lack of secondary products. DSC is also used to measure various thermal parameters of materials [49]. The glass transition (T_g) and melting (T_m) temperatures for polymers **4–6** were determined from the DSC measurements (Table 4, Figure 3). According to these results, we concluded that polymers **4–6** are amorphous and thermally stable materials at a temperature up to 290 °C and have endothermic peaks.

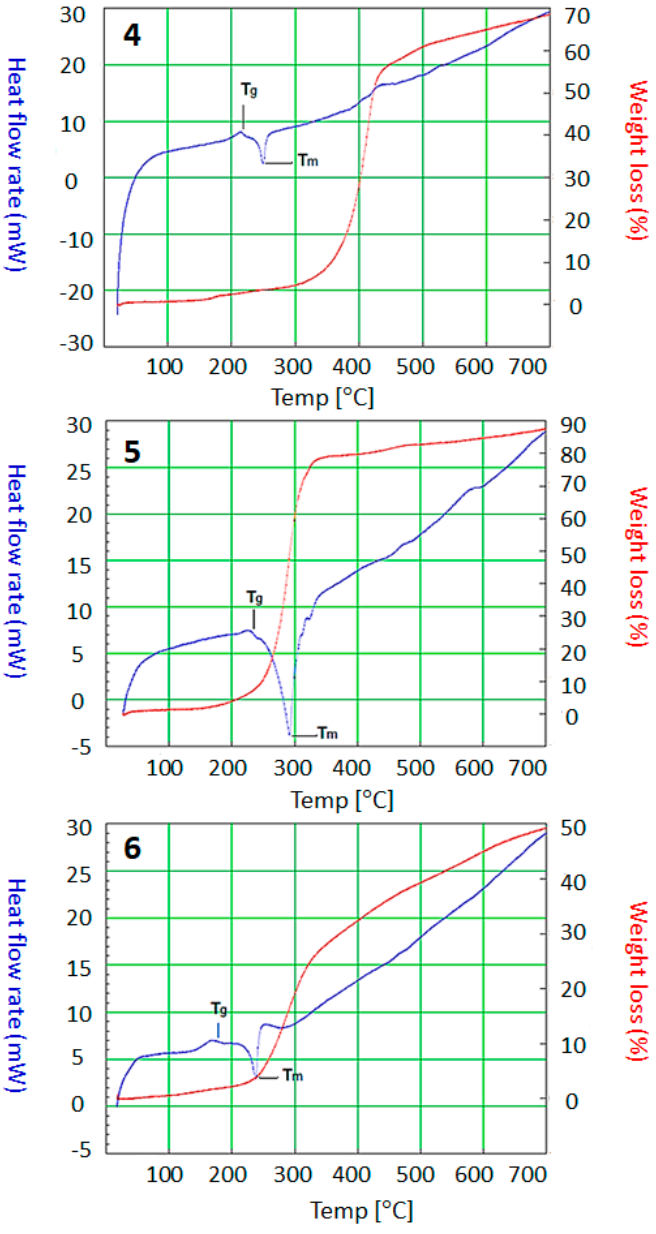

Figure 3. TGA and differential scanning calorimetry (DSC) spectra of polymers **4–6**.

Table 4. T_g, T_m, and weight loss temperatures of polymers **4–6**.

Polymer	DSC		TGA
	T_g (°C)	T_m (°C)	Weight Loss Temperature (°C)
4	220	253	400
5	225	290	295
6	175	245	285

3.5. Surface Area and Porosity of Polymers **4–6**

The BET method is generally used to estimate the surface area of the examined adsorbents [50,51]. The collected data are displayed in the form of a N_2 adsorption isotherm, which is obtained by plotting the quantity of the adsorbed gas against the relative pressure. The N_2 adsorption–desorption measurements of polymers **4–6** at 77 K were of type III with no single-layer adsorption and their average pore diameter and total volume were less than 2 nm (i.e., microporous materials) and 0.015–0.034 cm^3 g^{-1}, respectively (Table 5). The N_2 adsorption–desorption and pore size distribution isotherms of polymers **4–6** are shown in Figures 4 and 5. The BET surface area (S_{BET}) of polymers **4**, **5**, and **6** was relatively low (Table 5). Clearly, both the surface area and pore volume of polymers **4–6** are lower compared with those for activated carbons [52].

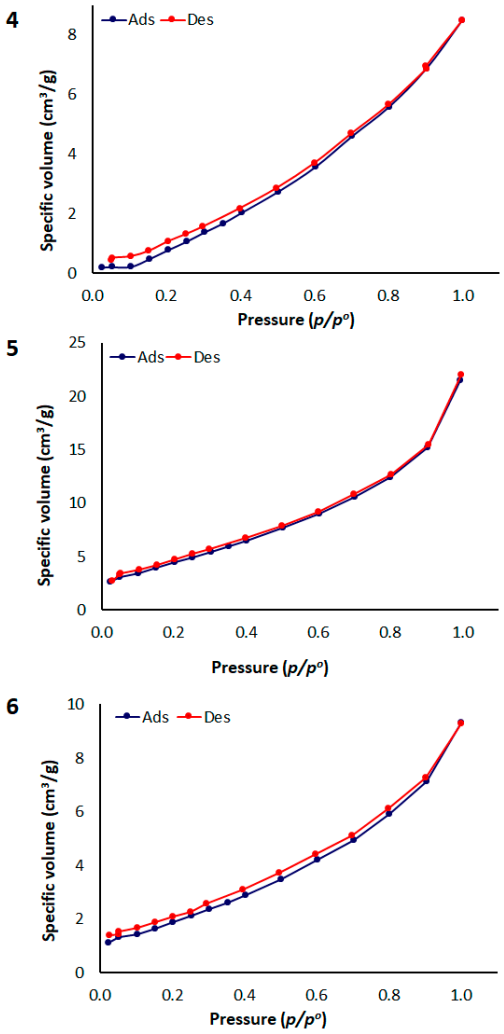

Figure 4. N_2 adsorption–desorption of polymers **4–6**.

Table 5. Textural properties of polymers **4–6**.

Polymer	S_{BET} (m^2 g^{-1}) [a]	Total Volume (cm^3 g^{-1}) [b]	Pore Size (nm) [c,d]
4	12.112	0.016	1.950
5	18.012	0.034	1.952
6	8.174	0.015	1.947

[a] S_{BET} was calculated from the N_2 adsorption isotherms using the BET method. [b] The total pore volume was calculated at p/p° = 0.98. [c] Average pore diameter. [d] Adsorption and desorption were carried out in the same conditions.

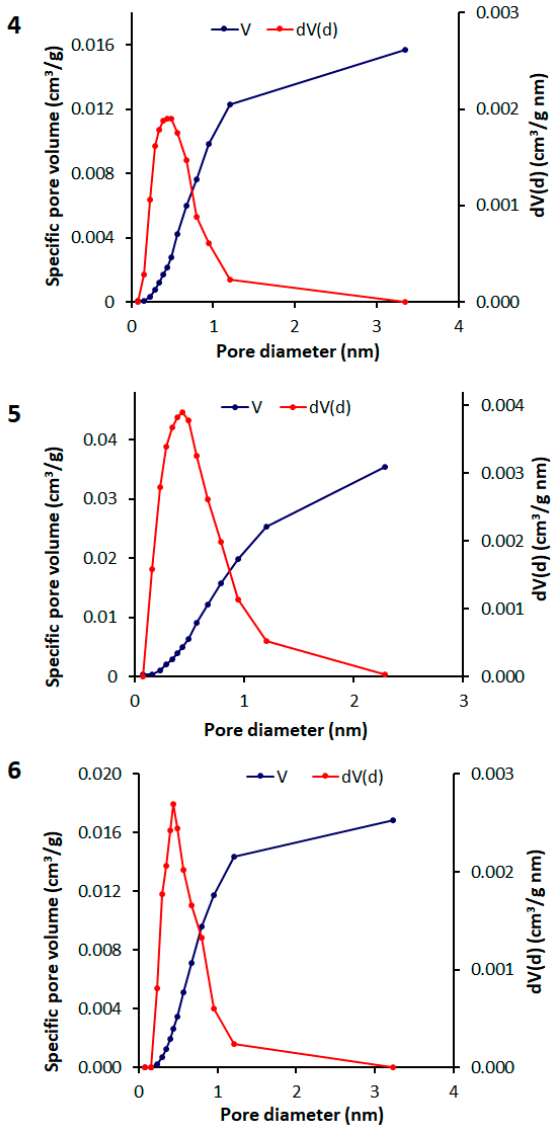

Figure 5. Pore size distribution isotherms of polymers **4–6**.

Porous materials are often described based on the size of the pores. However, the reported average pore size cannot be used to describe the porosity of the synthesized polymers. The synthesized POPs have mainly microporous structures, along with mesoporous, macroporous, and other materials.

*3.6. CO_2 Adsorption of Polymers **4–6***

The CO_2 adsorption of polymers **4–6** was investigated at 323 K and 40 bar. High temperature and pressure were used in order to maximize the CO_2 uptake by polymers based on our previous work [40–43]. The CO_2 adsorption isotherms for the adsorbed CO_2 within the polymer pores under

the applied temperature (323 K) and pressure (40 bar) conditions are shown in Figure 6. Polymers **4–6** showed a reasonable CO_2 uptake in the range of 11.295–30.581 $cm^3\ g^{-1}$ (Table 6), while polymer **5** with the *meta*-arrangement exhibited the highest CO_2 uptake (6.0 wt%), probably due to its relatively high surface area (18.012 $m^2\ g^{-1}$) and total pore volume (0.034 $cm^3\ g^{-1}$) compared to the other two polymers with *ortho*- and *para*-arrangements. Similar findings have been reported for polyphosphates containing 1,4-diaminobenzene and benzidine [41,42]. It was thus clearly indicated that the pore size distribution and surface area can affect the CO_2 storage capacity of polymers **4–6** under the applied conditions. Since these parameters are probably mainly controlled by the geometry of the polymer building blocks, the higher CO_2 adsorption capacity of **5** could also be explained.

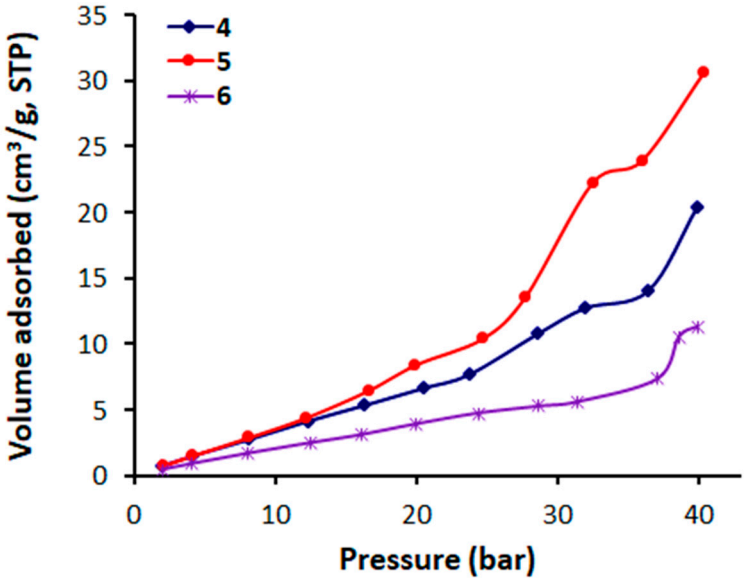

Figure 6. CO_2 adsorption isotherms of polymers **4–6**.

Table 6. CO_2 adsorption capacity of polymers **4–6** at 323 K and 40 bar.

Polymer	CO_2 Uptake		
	$cm^3\ g^{-1}$ [a]	$mmol\ g^{-1}$ [b]	Wt %
4	20.418	0.910	4.0
5	30.581	1.364	6.0
6	11.295	0.503	2.2

[a] The volume occupied of adsorbed CO_2 per gram at the thermodynamic state. [b] The millimoles of the adsorbed gas per gram of the substance.

The adsorbent–adsorbate interactions were relatively weak and the gas was clustered around the –CH=N group within the polymer surface [53]. The surface area of polymeric materials is not the only contributing factor to the adsorption of CO_2. However, polar groups such as –CH=N, –OH, NH_2, and O=C–NH within the skeleton of the POPs can lead to a high CO_2 uptake by tuning the isoelectric head of adsorption [54–58].

The storage capacity of POPs **4–6** was also comparable to that reported for metal complexes containing valsartan [39], and telmisartan [40], and for polyphosphates containing 1,4-diamainobenzene [41]. Instead, polyphosphates consisting of benzidine [42] and melamine Schiff bases [43] showed better CO_2 uptake than **4–6**, possibly due to the tunable pore size of their particles and the presence of functional groups. Nevertheless, in this case, it should be considered that a direct comparison between phosphate- and silicate-containing polymers is difficult. The newly synthesized POPs are easy to produce, have high thermal stability, and their surface area and pore

structures can be tuned to maximize CO_2 uptake. Therefore, these materials have potential to be used in gas capture applications.

4. Conclusions

Three silicon-containing POPs with *ortho*-, *meta*-, and *para*-arrangements were synthesized and their structures and properties were established. The synthesized porous polymers had different properties and adsorption capacity toward CO_2 due to their different surface area and pore size distribution. Among the synthesized POPs, the *meta*-arranged polymer (**5**) exhibited the highest CO_2 uptake, as it had a relatively high surface area and pore total volume compared to polymers **4** and **6**.

Supplementary Materials: The following are available online at http://www.mdpi.com/2227-9717/8/11/1488/s1, Figure S1: FTIR spectrum of **1**; Figure S2: FTIR spectrum of **2**; Figure S3: FTIR spectrum of **3**; Figure S4: ^{1}H NMR spectrum of **1**; Figure S5: ^{1}H NMR spectrum of **2**; Figure S6: ^{1}H NMR spectrum of **3**; Figure S7: ^{13}C NMR spectrum of **2**; Figure S8: FTIR spectrum of **4**; Figure S9: FTIR spectrum of **5**; Figure S10: FTIR spectrum of **6**; Figure S11: EDX of **4**; Figure S12: EDX of **5**; Figure S13: EDX of **6**; Figure S14: FESEM of **4**; Figure S15: FESEM of **5**; Figure S16: FESEM of **6**.

Author Contributions: Conceptualization and experimental design: A.S.H., E.Y., M.H.A., D.S.A., and G.A.E.-H.; Experimental work and data analysis: S.H.M.; writing: E.Y., D.S.A., and G.A.E.-H. All authors have read and agreed to the published version of the manuscript.

Funding: The authors are grateful to the Deanship of Scientific Research, King Saud University for funding through Vice Deanship of Scientific Research Chairs.

Acknowledgments: We thank Al-Nahrain and Tikrit Universities for technical support.

Conflicts of Interest: The authors declare that they have no conflict of interest.

References

1. Kweku, D.W.; Bismark, O.; Maxwell, A.; Desmond, K.A.; Danso, K.B.; Oti-Mensah, E.A.; Quachie, A.T.; Adormaa, B.B. Greenhouse effect: Greenhouse gases and their impact on global warming. *J. Sci. Res. Rep.* **2017**, *17*, 39630. [CrossRef]
2. Singh, U. Carbon capture and storage: An effective way to mitigate global warming. *Curr. Sci.* **2013**, *105*, 914–922.
3. Wang, X.P.; Yu, J.J.; Cheng, J.; Hao, J.P.; Xu, Z.P. High-temperature adsorption of carbon dioxide on mixed oxides derived from hydrotalcite-like compounds. *Environ. Sci. Technol.* **2008**, *42*, 614–618. [CrossRef]
4. Bui, M.; Adjiman, C.S.; Bardow, A.; Anthony, E.J.; Boston, A.; Brown, S.; Fennell, P.S.; Fuss, S.; Galindo, A.; Hackett, L.A.; et al. Carbon capture and storage (CCS): The way forward. *Energy Environ. Sci.* **2018**, *11*, 1062–1176. [CrossRef]
5. De Coninck, H.; Benson, S.M. Carbon dioxide capture and storage: Issues and prospects. *Annu. Rev. Environ. Resour.* **2014**, *39*, 243–270. [CrossRef]
6. Leunga, D.Y.C.; Caramanna, G.; Maroto-Valerb, M. An overview of current status of carbon dioxide capture and storage technologies. *Renew. Sustain. Energy Rev.* **2014**, *39*, 426–443. [CrossRef]
7. D'Alessandro, D.M.; Smit, B.; Long, J.R. Carbon dioxide capture: Prospects for new materials carbon dioxide capture: Prospects for new materials. *Angew. Chem. Int. Ed.* **2010**, *49*, 6058–6082. [CrossRef]
8. Rochelle, G.T. Amine scrubbing for CO_2 capture. *Science* **2009**, *325*, 1652–1654. [CrossRef]
9. Electric Power Research Institute. *Program on Technology Innovation: Post-Combustion CO_2 Capture Technology Development*; Electric Power Research Institute: Palo Alto, CA, USA, 2008.
10. Abu-Khader, M.M. Recent progress in CO_2 capture/sequestration: A review. *Energy Sources Part A* **2006**, *28*, 1261–1279. [CrossRef]
11. Smiglak, M.; Metlen, A.; Rogers, R.D. The second evolution of ionic liquids: From solvents and separations to advanced materials—Energetic examples from the ionic liquid cookbook. *Acc. Chem. Res.* **2007**, *40*, 1182–1192. [CrossRef]
12. Bates, E.D.; Mayton, R.D.; Ntai, I.; Davis, J.H. CO_2 capture by a task-specific ionic liquid. *J. Am. Chem. Soc.* **2002**, *124*, 926–927. [CrossRef] [PubMed]

13. Lee, K.B.; Beaver, M.G.; Caram, H.S.; Sircar, S. Reversible chemisorbents for carbon dioxide and their potential applications. *Ind. Eng. Chem. Res.* **2008**, *47*, 8048–8062. [CrossRef]
14. Choi, S.; Drese, J.H.; Jones, C.W. Adsorbent materials for carbon dioxide capture from large anthropogenic point sources. *ChemSusChem* **2009**, *2*, 796–854. [CrossRef] [PubMed]
15. Hicks, J.C.; Drese, J.H.; Fauth, D.J.; Gray, M.L.; Qi, G.; Jones, C.W. Designing adsorbents for CO_2 capture from flue gas-hyperbranched aminosilicas capable of capturing CO_2 reversibly. *J. Am. Chem. Soc.* **2008**, *130*, 2902–2903. [CrossRef] [PubMed]
16. Dawson, R.; Cooper, A.I.; Adams, D.J. Nanoporous organic polymer networks. *Prog. Polym. Sci.* **2012**, *37*, 530–563. [CrossRef]
17. Henis, J.M.S. Commercial and Practical Aspects of Gas Separation Membranes. In *Polymeric Gas Separation Membranes*; Paul, D.R., Yampol'skii, Y.P., Eds.; CRC Press: Boca Raton, FL, USA, 1994.
18. Wu, D.; Xu, F.; Sun, B.; Fu, R.; He, H.; Matyjaszewski, K. Design and preparation of porous polymers. *Chem. Rev.* **2012**, *112*, 3959–4015. [CrossRef]
19. Xu, Y.; Jin, S.; Xu, H.; Nagai, A.; Jiang, D. Conjugated microporous polymers: Design, synthesis and application. *Chem. Soc. Rev.* **2013**, *42*, 8012–8031. [CrossRef]
20. Jones, J.T.A.; Hasell, T.; Wu, X.; Bacsa, J.; Jelfs, K.E.; Schmidtmann, M.; Chong, S.Y.; Adams, D.J.; Trewin, A.; Schiffman, F.; et al. Modular and predictable assembly of porous organic molecular crystals. *Nature* **2011**, *474*, 367–371. [CrossRef]
21. Kumar, A.; Madden, D.G.; Lusi, M.; Chen, K.-J.; Daniels, E.A.; Curtin, T.; Perry, J.J., IV; Zaworotko, M.J. Direct air capture of CO_2 by physisorbent materials. *Angew. Chem. Int. Ed.* **2015**, *54*, 14372–14377. [CrossRef]
22. Xiang, Z.; Mercado, R.; Huck, J.M.; Wang, H.; Guo, Z.; Wang, W.; Cao, D.; Haranczyk, M.; Smit, B. Systematic tuning and multifunctionalization of covalent organic polymers for enhanced carbon capture. *J. Am. Chem. Soc.* **2015**, *137*, 13301–13307. [CrossRef]
23. Lau, C.H.; Konstas, K.; Thornton, A.W.; Liu, A.C.Y.; Mudie, S.; Kennedy, D.F.; Howard, S.C.; Hill, A.J.; Hill, M.R.G. Gas-separation membranes loaded with porous aromatic frameworks that improve with age. *Angew. Chem. Int. Ed.* **2015**, *54*, 2669–2673. [CrossRef] [PubMed]
24. Sun, Q.; Dai, Z.; Meng, X.; Wang, L.; Xiao, F.-S. Task-specific design of porous polymer heterogeneous catalysts beyond homogeneous counterparts. *ACS Catal.* **2015**, *5*, 4556–4567. [CrossRef]
25. Ahmed, D.S.; El-Hiti, G.A.; Yousif, E.; Ali, A.A.; Hameed, A.S. Design and synthesis of porous polymeric materials and their applications in gas capture and storage: A review. *J. Polym. Res.* **2018**, *25*, 75. [CrossRef]
26. Choi, J.H.; Choi, K.M.; Jeon, H.J.; Choi, Y.J.; Lee, Y.; Kang, J.K. Acetylene gas mediated conjugated microporous polymers (ACMPs): First use of acetylene gas as a building unit. *Macromolecules* **2010**, *43*, 5508–5511. [CrossRef]
27. Jiang, J.-X.; Trewin, A.; Adams, D.J.; Cooper, A.I. Band gap engineering in fluorescent conjugated microporous polymers. *Chem. Sci.* **2011**, *2*, 1777–1781. [CrossRef]
28. Yuan, D.; Lu, W.; Zhao, D.; Zhou, H.-C. Highly stable porous polymer networks with exceptionally high gas-uptake capacities. *Adv. Mater.* **2011**, *23*, 3723–3725. [CrossRef]
29. Wang, D.; Xue, L.; Li, L.; Deng, B.; Feng, S.; Liu, H.; Zhao, X. Rational design and synthesis of hybrid porous polymers derived from polyhedral oligomeric silsesquioxanes *via* Heck coupling reactions. *Macromol. Rapid Commun.* **2013**, *34*, 861–866. [CrossRef]
30. Dawson, R.; Stockel, E.; Holst, J.R.; Adams, D.J.; Cooper, A.I. Microporous organic polymers for carbon dioxide capture. *Energy Environ. Sci.* **2011**, *4*, 4239–4245. [CrossRef]
31. Panek, R.; Wdowin, M.; Franus, W.; Czarna, D.; Stevens, L.A.; Deng, H.; Liu, J.; Sun, C.; Liu, H.; Snape, C.E. Fly ash-derived MCM-41 as a low-cost silica support for polyethyleneimine in post-combustion CO_2 capture. *J. CO_2 Util.* **2017**, *22*, 81–90. [CrossRef]
32. Chaubey, R.; Sahu, S.; James, O.O.; Maity, S. A review on development of industrial processes and emerging techniques for production of hydrogen from renewable and sustainable sources. *Renew. Sustain. Energy Rev.* **2013**, *23*, 443–462. [CrossRef]
33. Hosseini, S.E.; Wahid, M.A. Hydrogen production from renewable and sustainable energy resources: Promising green energy carrier for clean development. *Renew. Sustain. Energy Rev.* **2016**, *57*, 850–866. [CrossRef]

34. Moliner, R.; Lázaro, M.J.; Suelves, I. Analysis of the strategies for bridging the gap towards the hydrogen economy. *Int. J. Hydrog. Energy* **2016**, *41*, 19500–19508. [CrossRef]
35. Pudukudy, M.; Yaakob, Z.; Mohammad, M.; Narayanan, B.; Sopian, K. Renewable hydrogen economy in Asia–opportunities and challenges: An overview. *Renew. Sustain. Energy Rev.* **2014**, *30*, 743–757. [CrossRef]
36. Lim, K.L.; Liu, Y.; Zhang, Q.-A.; Chan, S.L.I. Effects of partial substitutions of cerium and aluminum on the hydrogenation properties of La(0.65-x)CexCa1.03Mg1.32Ni(9-y)Aly alloy. *Int. J. Hydrog. Energy* **2014**, *39*, 10537–10545. [CrossRef]
37. Ren, J.; Musyoka, N.M.; Langmi, H.W.; North, B.C.; Mathe, M.; Kang, X.; Liao, S. Hydrogen storage in Zr-fumarate MOF. *Int. J. Hydrog. Energy* **2015**, *40*, 10542–10546. [CrossRef]
38. Najim, L.H.; El-Hiti, G.A.; Ahmed, D.S.; Mohammed, A.; Alotaibi, M.H.; Yousif, E. Valsartan metal complexes as capture and reversible storage media for methane. *Appl. Petrochem. Res.* **2020**, *10*. [CrossRef]
39. Mohammed, A.; Yousif, E.; El-Hiti, G.A. Synthesis and use of valsartan metal complexes as media for carbon dioxide storage. *Materials* **2020**, *13*, 1183. [CrossRef]
40. Hadi, A.G.; Jawad, K.; Yousif, E.; El-Hiti, G.A.; Alotaibi, M.H.; Ahmed, D.S. Synthesis of telmisartan organotin(IV) complexes and their use as carbon dioxide capture media. *Molecules* **2019**, *24*, 1631. [CrossRef]
41. Satar, H.A.; Ahmed, A.A.; Yousif, E.; Ahmed, D.S.; Alotibi, M.F.; El-Hiti, G.A. Synthesis of novel heteroatom-doped porous-organic polymers as environmentally efficient media for carbon dioxide storage. *Appl. Sci.* **2019**, *9*, 4314. [CrossRef]
42. Ahmed, D.S.; El-Hiti, G.A.; Yousif, E.; Hameed, A.S.; Abdalla, M. New eco-friendly phosphorus organic polymers as gas storage media. *Polymers* **2017**, *9*, 336. [CrossRef]
43. Omer, R.M.; Al-Tikrity, E.T.B.; El-Hiti, G.A.; Alotibi, M.F.; Ahmed, D.S.; Yousif, E. Porous aromatic melamine Schiff bases as highly efficient media for carbon dioxide storage. *Processes* **2020**, *8*, 17. [CrossRef]
44. Konno, M.; Ogashiwa, T.; Sunaoshi, T.; Orai, Y.; Sato, M. Lattice imaging at an accelerating voltage of 30 kV using an in-lens type cold field-emission scanning electron microscope. *Ultramicroscopy* **2014**, *145*, 28–35. [CrossRef] [PubMed]
45. Bates, S.; Zografi, G.; Engers, D.; Morris, K.; Crowley, K.; Newman, A. Analysis of amorphous and nanocrystalline solids from their X-ray diffraction patterns. *Pharm. Res.* **2006**, *23*, 2333–2349. [CrossRef] [PubMed]
46. Lattimer, B.Y.; Ouellette, J. Properties of composite materials for thermal analysis involving fires. *Compos. Part A Appl. Sci. Manuf.* **2006**, *37*, 1068–1081. [CrossRef]
47. Shyichuk, A.V.; White, J.R. Analysis of chain-scission and crosslinking rates on the photooxidation of polystyrene. *J. Appl. Polym. Sci.* **2000**, *77*, 3015–3023. [CrossRef]
48. Wampler, T.P. *Applied Pyrolysis Handbook*, 2nd ed.; CRC Press, Taylor and Francis: Boca Raton, FL, USA, 2006.
49. Lopes, C.M.A.; Felisberti, M.I. Thermal conductivity of PET/(LDPE/AI) composites determined by MDSC. *Polym. Test.* **2004**, *23*, 637–643. [CrossRef]
50. Srisuda, S.; Virote, B. Adsorption of formaldehyde vapor by amine-functionalized mesoporous silica materials. *J. Environ. Sci.* **2008**, *20*, 379–384. [CrossRef]
51. Rouquerol, J.; Rouquerol, F.; Sing, K.S.W.; Llewellyn, P.; Maurin, G. *Adsorption by Powders and Porous Solids: Principles, Methodology and Applications*, 2nd ed.; Academic Press: New York, NY, USA, 2014.
52. Kwiatkowski, M.; Fierro, V.; Celzard, A. Confrontation of various adsorption models for assessing the porous structure of activated carbons. *Adsorption* **2019**, *25*, 1673–1682. [CrossRef]
53. Thommes, M.; Kaneko, K.; Neimark, A.V.; Olivier, J.P.; Rodriguez-Reinoso, F.; Rouquerol, J.; Sing, K.S.W. Physisorption of gases, with special reference to the evaluation of surface area and pore size distribution (IUPAC Technical Report). *Pure Appl. Chem.* **2015**, *87*, 1051–1069. [CrossRef]
54. Suresh, V.M.; Bonakala, S.; Atreya, H.S.; Balasubramanian, S.; Maji, T.K. Amide functionalized microporous organic polymer (Am-MOP) for selective CO_2 sorption and catalysis. *ACS Appl. Mater. Interfaces* **2014**, *6*, 4630–4637. [CrossRef]
55. Xu, C.; Hedin, N. Synthesis of microporous organic polymers with high CO_2-over-N_2 selectivity and CO_2 adsorption. *J. Mater. Chem. A* **2013**, *1*, 3406–3414. [CrossRef]
56. Dawson, R.; Cooper, A.I.; Adams, D.J. Chemical functionalization strategies for carbon dioxide capture in microporous organic polymers. *Polym. Int.* **2013**, *62*, 345–352. [CrossRef]

57. Song, W.-C.; Xu, X.-K.; Chen, Q.; Zhuang, Z.-Z.; Bu, X.-H. Nitrogen-rich diaminotriazine-based porous organic polymers for small gas storage and selective uptake. *Polym. Chem.* **2013**, *4*, 4690–4696. [CrossRef]
58. Jeon, H.J.; Choi, J.H.; Lee, Y.; Choi, K.M.; Park, J.H.; Kang, J.K. Highly selective CO_2-capturing polymeric organic network structures. *Adv. Energy Mater.* **2012**, *2*, 225–228. [CrossRef]